

PAPER • OPEN ACCESS

## Brain network dynamics fingerprints are resilient to data heterogeneity

To cite this article: Tommaso Menara *et al* 2021 *J. Neural Eng.* **18** 026004

View the [article online](#) for updates and enhancements.



## PAPER

## Brain network dynamics fingerprints are resilient to data heterogeneity

## OPEN ACCESS

## RECEIVED

7 October 2020

## REVISED

3 December 2020

## ACCEPTED FOR PUBLICATION

23 December 2020

## PUBLISHED

24 February 2021

Original Content from this work may be used under the terms of the [Creative Commons Attribution 4.0 licence](#).

Any further distribution of this work must maintain attribution to the author(s) and the title of the work, journal citation and DOI.

Tommaso Menara<sup>1,2</sup> , Giuseppe Lisi<sup>3,4</sup> , Fabio Pasqualetti<sup>2</sup>  and Aurelio Cortese<sup>1</sup> <sup>1</sup> Computational Neuroscience Laboratories, ATR Institute International, Kyoto, Japan<sup>2</sup> Department of Mechanical Engineering, University of California at Riverside, Riverside, CA, United States of America<sup>3</sup> Nagoya Institute of Technology, Nagoya, Japan<sup>4</sup> Brain Information Communication Research Laboratory, ATR Institute International, Kyoto, JapanE-mail: [tomenara@engr.ucr.edu](mailto:tomenara@engr.ucr.edu) and [cortese.aurelio@gmail.com](mailto:cortese.aurelio@gmail.com)**Keywords:** neuroimaging, fMRI, multi-site studies, hidden Markov models, brain dynamics, reproducibility, traveling subjectsSupplementary material for this article is available [online](#)**Abstract**

*Context.* Large multi-site neuroimaging datasets have significantly advanced our quest to understand brain-behavior relationships and to develop biomarkers of psychiatric and neurodegenerative disorders. Yet, such data collections come at a cost, as the inevitable differences across samples may lead to biased or erroneous conclusions. *Objective.* We aim to validate the estimation of individual brain network dynamics fingerprints and appraise sources of variability in large resting-state functional magnetic resonance imaging (rs-fMRI) datasets by providing a novel point of view based on data-driven dynamical models. *Approach.* Previous work has investigated this critical issue in terms of effects on static measures, such as functional connectivity and brain parcellations. Here, we utilize dynamical models (hidden Markov models—HMM) to examine how diverse scanning factors in multi-site fMRI recordings affect our ability to infer the brain's spatiotemporal wandering between large-scale networks of activity. Specifically, we leverage a stable HMM trained on the Human Connectome Project (homogeneous) dataset, which we then apply to an heterogeneous dataset of traveling subjects scanned under a multitude of conditions. *Main Results.* Building upon this premise, we first replicate previous work on the emergence of non-random sequences of brain states. We next highlight how these time-varying brain activity patterns are robust subject-specific fingerprints. Finally, we suggest these fingerprints may be used to assess which scanning factors induce high variability in the data. *Significance.* These results demonstrate that we can (i) use large scale dataset to train models that can be then used to interrogate subject-specific data, (ii) recover the unique trajectories of brain activity changes in each individual, but also (iii) urge caution as our ability to infer such patterns is affected by how, where and when we do so.

**1. Introduction**

Untangling the brain's dynamics at rest is a central aspect in the quest to reveal the mechanisms underlying the spontaneous wandering of the mind between well-established, large-scale networks of neural activity [1–3]. The characterization of the brain dynamics' spatiotemporal organization into networks has greatly benefited from the creation of very large neuroimaging datasets [4, 5], such as the Human Connectome Project (HCP) [6, 7], the UK

Biobank [8], and, in the context of neurodegenerative diseases, the Alzheimer's Disease Neuroimaging Initiative [9]. Large neuroimaging datasets have, furthermore, played a crucial role in the development of novel biomarkers for psychiatric and neurodegenerative disorders [10–12]. Yet, appraising how differences in physical parameters or scanning protocols affect the quality of these data—especially fMRI recordings—remains an outstanding problem [13–16]. For instance, imaging sequences are considerably affected by site-dependent differences such as

scanner drift over time, or maintenance routine [16]. Only few recent works have addressed the problem of data variability in rs-fMRI data across sites [17–20], while some others have proposed techniques to harmonize multi-site data [10, 12, 14, 16, 21, 22]. Despite growing interest in the intricacies inherent to multi-site data, this line of research is still in its infancy (the first publication appeared in 2013 [23]). Furthermore, although the brain is a complex dynamical system capable of exhibiting rich non-linear dynamics [24, 25], most studies to date have relied on static measures (e.g. functional connectivity); and little to no attempts exist at exploring such issues from the viewpoint of dynamical models.

Data-driven dynamical models are a promising and powerful tool for the analysis and prediction of the spatiotemporal organization of brain activity [26–29]. These models allow us to harness the vast amount of spurious information contained in large datasets [30–32], capture the hierarchical organization of brain activity [33], enhance brain-computer interfaces [34, 35], and may even be employed in clinical settings [10, 36–38]. However, how the inference and identification of dynamical models is affected by different factors in multi-site data acquisition has yet to be investigated. Additionally, dynamical models could provide fine-grained insight into the extent of the effect of these factors on the data.

One limitation of data-driven models is that, generally, large amounts of data are needed to train the model in the first place. Here, we avoid this issue by employing two datasets. We leverage the high number of subjects ( $n_{\text{HCP}} > 1000$ ) with rs-fMRI data available in the HCP dataset [6], to train a stable and reliable hidden Markov model (HMM). An HMM infers brain network dynamics from rs-fMRI time series, where networks are probability distributions representing graphs. We then apply the pretrained HMM to the smaller ( $n_{\text{TS}} = 9$ ) Traveling-subject dataset, which consists of a novel, state-of-the-art collection of rs-fMRI measurements of nine healthy subjects who traveled to twelve different sites and were scanned under various conditions (different sites, days, phase encoding, number of channels/coils, manufacturer, scanner; see section 2 and supplementary table 1 (available online at [stacks.iop.org/JNE/18/026004/mmedia](https://stacks.iop.org/JNE/18/026004/mmedia)) for a full list of scanning factors and attributes) [22]. This way, we were able to infer subject-specific brain states and investigate how the retrieval of brain state time courses is affected by an array of scanning factors. Training the model on the HCP data guarantees that (i) the model is inferred on a large sample, made of carefully collected and homogeneous data, and that (ii) the model is stable and does not over-fit on a dataset of limited size. We illustrate the methodological approach in figure 1.

Thus, we first utilize the trained HMM to validate the findings on rs-fMRI fingerprints—robust

and reproducible quantitative signatures—reported in previous work [28, 33, 39]. We then generalize these findings by applying the HCP-trained HMM to the Traveling-subject dataset. This important step allows us to exploit the HMM to assess if, and to what extent, mixed scanning factors affect subject-specific fingerprints and, thus, rs-fMRI recordings. We depart from previous work, which has mostly relied on static functional connectivity/correlation measures and smaller datasets, by exploiting dynamical brain network collective states at a finer temporal resolution. Altogether, this paper juxtaposes complementary, yet contrasting, results with respect to rs-fMRI data analysis: we confirm previous findings reporting subject-specific fingerprints, but we also shed light on the presence of factors that induce variability in such fingerprints and, thus, the homogeneity of multi-site fMRI data collections and subsequent inference from the viewpoint of dynamical models.

## 2. Materials and methods

### 2.1. Datasets

The two dataset used in this study are (i) the HCP 1200-subject distribution (data available at <https://db.humanconnectome.org>) and (ii) the Traveling-subject dataset (data available at <https://bicyr-resource.atr.jp/srpbsts/> after free registration). The former consists of rs-fMRI data from  $N = 1206$  healthy subjects (age 22–35) that were scanned twice (two 15 min runs) on two different days, one week apart, on a Siemens 3 T Connectome-Skyra scanner. For each subject, in total four 15 min runs of rs-fMRI time series data with a temporal resolution of 0.72 s and a spatial resolution of 2 mm isotropic were available. For our analysis, we used time series from the 1003 subjects with four complete scanning sessions. The HCP dataset provides the required ethics and consent needed for study and dissemination, such that no further institutional review board (IRB) approval is required.

The Traveling-subject dataset consists of nine healthy subjects (all men; age range 24–32; mean age  $27 \pm 2.6$  yr), who were all scanned at each of the 12 sites, producing a total of 411 10 min scanning sessions [22]. Each participant underwent three rs-fMRI sessions of 10 min each at nine sites, two sessions of 10 min each at two sites (HKH and HUH), and five cycles (morning, afternoon, following day, following week, and following month) consisting of three 10 min sessions each at a single site (ATT). In the latter situation, one participant underwent four rather than five sessions at the ATT site because of a poor physical condition. Thus, a total of 411 sessions were conducted ( $8 \text{ participants} \times (3 \times 9 + 2 \times 2 + 5 \times 3 \times 1) + 1 \text{ participant} \times (3 \times 9 + 2 \times 2 + 4 \times 3 \times 1)$ ) (see supplementary table 1 for all the details on the scanning protocols). In

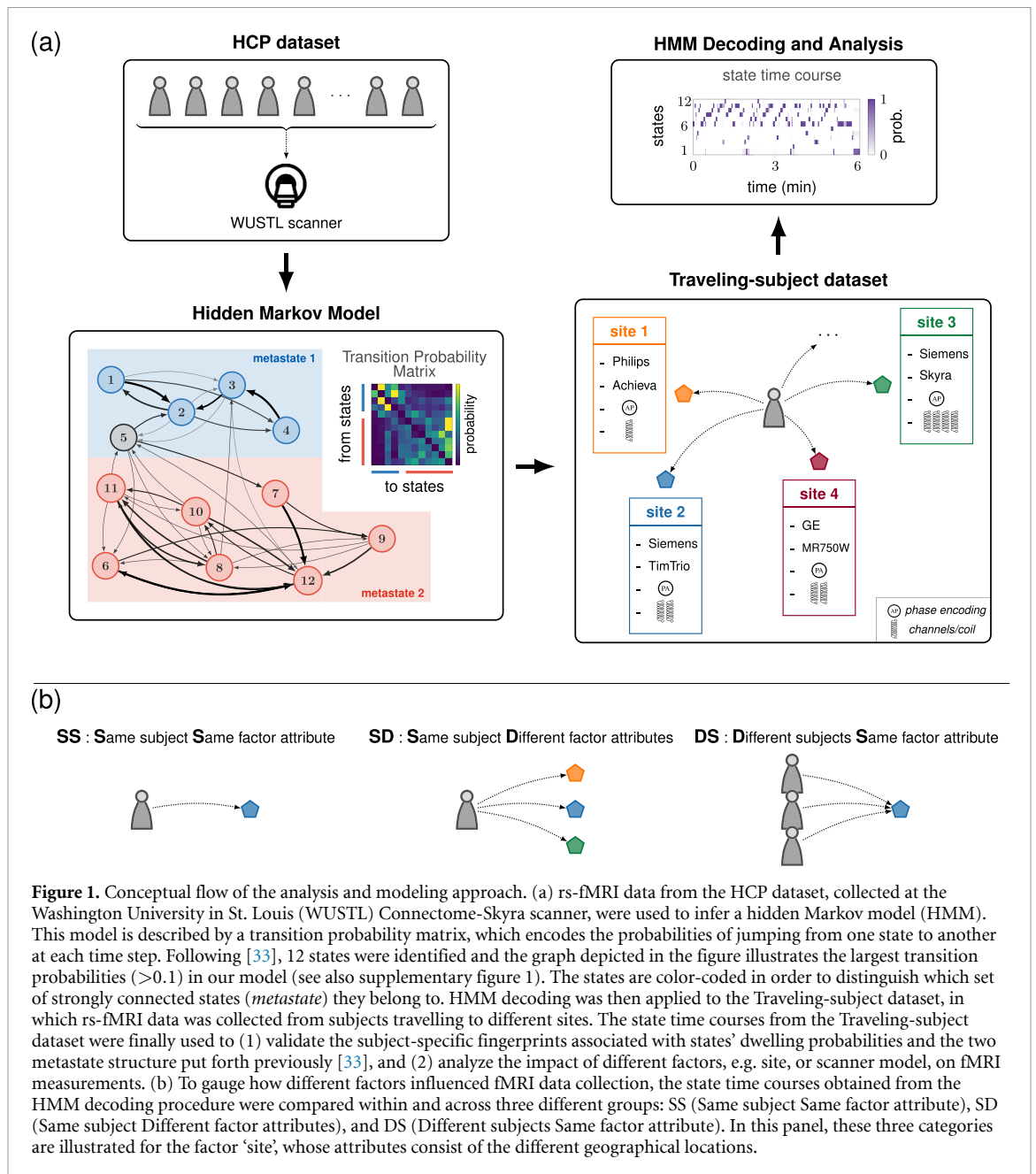


**Figure 1.** Conceptual flow of the analysis and modeling approach. (a) rs-fMRI data from the HCP dataset, collected at the Washington University in St. Louis (WUSTL) Connectome-Skyra scanner, were used to infer a hidden Markov model (HMM). This model is described by a transition probability matrix, which encodes the probabilities of jumping from one state to another at each time step. Following [33], 12 states were identified and the graph depicted in the figure illustrates the largest transition probabilities ( $>0.1$ ) in our model (see also supplementary figure 1). The states are color-coded in order to distinguish which set of strongly connected states (*metastate*) they belong to. HMM decoding was then applied to the Traveling-subject dataset, in which rs-fMRI data was collected from subjects travelling to different sites. The state time courses from the Traveling-subject dataset were finally used to (1) validate the subject-specific fingerprints associated with states' dwelling probabilities and the two metastate structure put forth previously [33], and (2) analyze the impact of different factors, e.g. site, or scanner model, on fMRI measurements. (b) To gauge how different factors influenced fMRI data collection, the state time courses obtained from the HMM decoding procedure were compared within and across three different groups: SS (Same subject Same factor attribute), SD (Same subject Different factor attributes), and DS (Different subjects Same factor attribute). In this panel, these three categories are illustrated for the factor 'site', whose attributes consist of the different geographical locations.

total, there were two phase-encoding directions (posterior to anterior ( $P \rightarrow A$ ) and anterior to posterior ( $A \rightarrow P$ )), three MRI manufacturers (Siemens, GE, and Philips), four numbers of channels per coil (8, 12, 24, and 32), and seven scanner types (TimTrio, Verio, Skyra, Spectra, MR750W, SignaHDxt, and Achieva). All participants in all datasets provided written informed consent. All recruitment procedures and experimental protocols were approved by the institutional review boards of the principal investigators' respective institutions (Advanced Telecommunications Research Institute International (ATR) (approval numbers: 13-133, 14-133, 15-133, 16-133, 17-133, and 18-133), Hiroshima University (E-38), Kyoto Prefectural University of Medicine (KPM) (RBMR-C- 1098), SWA (B-2014-019 and UMIN000016134), the University of Tokyo (UTO)

Faculty of Medicine (3150), Kyoto University (C809 and R0027), and Yamaguchi University (H23-153 and H25-85)) and conducted in accordance with the Declaration of Helsinki.

## 2.2. Hidden Markov model

In this work, we utilized HMM(s) to capture the dynamical evolution of brain states in subjects scanned at rest. In neuroscience and neuroimaging, HMMs are typically used to represent the stochastic relationship between a finite number of hidden states that underlie the brain's complex dynamics, whose evolution in time is captured by the measured data. That is, HMM is a powerful technique that enables the description of time series extracted from a system of interest. The underlying assumption of this class of models is that the observed time series of data

can be explained by a discrete sequence of hidden states, which must be finite in number. Additionally, to describe a HMM, an observation model needs to be chosen. We assume multivariate Gaussian observation model, so that, if  $\mathbf{x}_t$  denotes the data at time step  $t$ , and  $s_t$  represents the state at time step  $t$ , we can write, whenever state  $k$  is active,

$$\mathbf{x}_t | s_t \sim \text{multivariate Gaussian}(\boldsymbol{\mu}_k, \boldsymbol{\Sigma}_k)$$

where  $\boldsymbol{\mu}_k \in \mathbb{R}^c$  is the vector of the mean blood oxygen level-dependent (BOLD) activation for each channel, with  $c$  being the number of channels in the data, and  $\boldsymbol{\Sigma}_k \in \mathbb{R}^{c \times c}$  is the covariance matrix encoding the variances and covariances between channels. The transitions between different brain states depend on which state is active at the previous time step. Specifically, the probability of a state being active at time  $t$  depends on which state is active at time step  $t - 1$ . This is encoded in the Transition Probability Matrix (TPM)  $\Theta$ , in which the entry  $\Theta_{ij}$ —the transition probability—denotes the probability of state  $i$  becoming active at the next time step if state  $j$  is currently active. Formally, by denoting a probability with  $\Pr$ , we have that

$$\Pr(s_t = i) = \sum_j \Theta_{ij} \Pr(s_{t-1} = j)$$

For large datasets, it is possible to resort to stochastic Variational Bayes inference to estimate the posterior distribution of each state ( $\boldsymbol{\mu}_k, \boldsymbol{\Sigma}_k$ ), the probability of each state being active at each time step, and the transition probabilities between each pair of states  $\Theta_{ij}$  [31]. Finally, notwithstanding the fact that in this study the model has been inferred by concatenating all the subjects—thus implicitly defining the brain states as the outcome of common brain dynamics—the state time courses are subject-specific. That is, the states are inferred at the group level, but the time instants at which each brain state becomes active is subjective and changes between and across subjects.

## 2.3. Data preparation and HMM training

### 2.3.1. HCP dataset

Following [33], extensively preprocessed HCP ICA time series were used for the model training. The preprocessing followed the steps of [6, 40] and is briefly described here. Spatial preprocessing used the procedure described by [41]. Next, structured artifact removal using ICA was followed by FMRIB's ICA-based X-noisefier (FIX) from the FMRIB Software Library (FSL) [42], which removed more than 99% of the artifactual ICA components in the dataset. Finally, the 50 dimensional extensively preprocessed time series obtained after group spatial ICA are freely available at [www.humanconnectome.org/study/hcp-young-adult/document/extensively-processed-fmri-data-documentation](http://www.humanconnectome.org/study/hcp-young-adult/document/extensively-processed-fmri-data-documentation).

### 2.3.2. Traveling-subject dataset

The dataset was obtained from <https://bicr-resource.atr.jp/srpbsts/>. Hereafter, we describe the preprocessing procedure that was originally reported in [22]. Raw BOLD signals were preprocessed using SPM8, implemented in MATLAB (R2016b; Mathworks, Natick, MA, USA), The first 10 s of each scan data were discarded to account for T1 calibration. Ensuing preprocessing steps included: slice-timing correction, realignment, coregistration, segmentation of T1-weighted structural images, normalization to Montreal Neurological Institute (MNI) space, and spatial smoothing with an isotropic Gaussian kernel of 6 mm full-width at half-maximum. Thirty-six noise parameters were included in a linear regression model to remove multiple sources of spurious variance (e.g. six motion parameters, average signals over the whole brain, white matter, and cerebrospinal fluid) [43]. Time-series were band-pass filtered using a first-order Butterworth filter (0.01 Hz–0.08 Hz) to restrict the analysis to low-frequency fluctuations, which are characteristic of rs-fMRI BOLD activity [43]. Finally, to reduce the impact of head motion, scrubbing was performed: framewise displacement (FD) was calculated and volumes with  $\text{FD} > 0.5$  mm were removed [44]. Thus,  $5.4\% \pm 10.6\%$  volumes (mean (approximately 13 volumes)  $\pm 1$  SD) were removed per 10 min of rs-fMRI scanning (240 volumes). If the number of volumes removed after scrubbing exceeded the average of  $-3$  SD across participants, the sessions were excluded from the analysis. As a result, 14 sessions were removed from the dataset.

Before combining the HCP time series and the Traveling-subject time series for the model inference, we matched the temporal resolution of the two datasets. Specifically, for all results reported in the main text, the Traveling-subject time series were up-sampled in order to match the same repetition time as the HCP data (from  $\text{TR} = 2.5$  s to  $\text{TR} = 0.72$  s). We also down-sampled the HCP data from  $\text{TR} = 0.72$  s to  $\text{TR} = 2.5$  s to match the Traveling-subject repetition time. However, the model inferred on HCP down-sampled ICA time-series was not satisfactory (see below). Therefore, we have chosen to re-sample the Traveling-subject data instead of down-sampling the HCP data.

The HMM inference was performed on 50 dimensional standardized ICA time series (0 mean and unitary standard deviation) concatenated along the time direction. To concatenate HCP rs-fMRI data and the ones from the Traveling-subject dataset, we proceeded as follows. First, we matched the voxel coordinates of the Traveling-subject data with the group average spatial maps from the group-ICA decomposition of the HCP time series. These spatial maps were extracted from the group average analysis across all the subjects of the S1200 release and are available on the HCP website:

[www.humanconnectome.org/study/hcp-young-adult/document/extensively-processed-fmri-data-documentation](http://www.humanconnectome.org/study/hcp-young-adult/document/extensively-processed-fmri-data-documentation). Because the spatial maps are in a gray-ordinate CIFTI format [41], we extracted the  $xyz$  coordinates in a standard stereotaxic space MNI152 by using a *mid-thickness* surface file for the surface vertices and the coordinate transformation matrix included in the CIFTI file. Next, we extracted the time series from the Traveling-subject data corresponding to the same  $xyz$  coordinates of the aforementioned spatial map in Matlab by using the ROI Signal Extractor provided by the toolbox DPABI [45]. Finally, the HCP group average spatial map allowed us to obtain the estimated 50 dimensional ICs for the Traveling-subject data from the extracted time series. To note, once the Traveling-subject rs-fMRI time series were reduced to 50 ICs, they matched the spatial dimension of the HCP data used to infer the HMM in [33]. Finally, to train our HMM, we used the publicly available toolbox HMM-MAR (<https://github.com/OHBA-analysis/HMM-MAR>) [46]. We inferred  $N = 50$  models with 12 states (the number of states was chosen based on previous work [33]) from random initializations, multiple priors, and different combinations of the available datasets. Specifically, we inferred  $N_{1200} = 28$  models inferred on time series from the 1200 subject HCP release only with random priors,  $N_{820} = 14$  models inferred on the 820 subject HCP release (a subset of the 1200 subject release, which was used in the original work on the HMM derived hierarchical organization of brain states [33]) with random priors, and  $N_{TS} = 8$  models inferred on the nine subjects of the Traveling-subject dataset using the best model inferred from HCP data only one as a prior, so that  $N_{1200} + N_{820} + N_{TS} = 50$ ). The selection of the best model (described below in detail) took into account both classical model evaluation methods and the definition of the metrics used in this study.

#### 2.4. FO correlation matrix and fingerprints computation

By applying (i.e. decoding) an HMM to a dataset with multiple subjects, we obtained the state time courses for each subject, from which it is possible to compute the vector of the fractional occupancy (FO) of every state for each subject. Stacking such vectors in a matrix yielded the FO Matrix  $\mathbf{R}$ , which is a (*no. of subjects*)  $\times$  (*no. of states*) matrix that encodes state dynamics similarities across subjects. Each element  $\mathbf{R}_{ij}$  of this matrix denotes the fraction of time spent by subject  $i$  in state  $j$ . Further, by taking the pairwise correlation of the columns of the FO Matrix  $\mathbf{R}$ , we obtained the (*no. of states*)  $\times$  (*no. of states*) FO Correlation Matrix

$$\mathbf{C} = \text{corr}(\mathbf{R}_{:,k}, \mathbf{R}_{:,l}),$$

where  $\mathbf{R}_{:,k}$  denotes the column vector of the FO of all subjects for the  $k$ th state. This matrix captured the

overall organization of brain dynamics across states, and its entries quantified the affinity between the FOs of each pair of states across all subjects. In other words, the FO correlation matrix highlighted the similarities and dissimilarities between brain states, and encoded the temporal characteristics of brain network dynamics. The organization of the FO correlation matrix revealed (both by visual inspection and by numerical investigation) the emergence of two groups of states, known as metastates. Metastates are distinct sets of functional network states that the brain has a propensity to cycle within, and have been shown to hierarchically group brain states into a 2-metastate structure [33].

We made use of the information encoded in the FO correlation matrix to calculate two different subject-specific metrics in the Traveling-subject data that were key in this study: the Metastate Profile (MP) Differences and the FO correlations. Loosely speaking, the former provided the difference between the time spent in the two distinct metastates that emerged in our model, compatibly with previous findings [33]. The latter provided the pairwise correlation between the FO vectors of different scanning runs. To derive these metrics, we first construct the MP matrix, whose entry  $(i, k)$  represents the FO of the second metastate (states 6–12) minus the FO of the first metastate (states 1–4) for the subject  $i$  during the scanning session  $k$ . We excluded state 5 from our analysis as it was uncorrelated from the other states, had the highest variance, and was previously shown to be associated with head motion in the scanner [33]. Formally, given the FO Matrix  $\mathbf{R}$  for the run  $k$ ,  $\text{MP}_{i,k}$  is computed as follows:

$$\text{MP}_{i,k} = \sum_{j=6}^{12} \mathbf{R}_{i,j} - \sum_{j=1}^{4} \mathbf{R}_{i,j}.$$

Then, the MP Difference between run  $k_1$  for subject  $i_1$  and run  $k_2$  for subject  $i_2$  reads as

$$\text{MP Difference} = |\text{MP}_{i_1,k_1} - \text{MP}_{i_2,k_2}|.$$

Instead, the FO Correlation between run  $k_1$  for subject  $i_1$  and run  $k_2$  for subject  $i_2$  is defined as

$$\text{FO Correlation} = \text{corr}(\mathbf{FO}_{i_1,k_1}, \mathbf{FO}_{i_2,k_2}),$$

where  $\mathbf{FO}_{i,k}$  denotes the 11-dimensional column vector of the FOs of all 12 states minus state 5 for subject  $i$  and run  $k$ .

It is worth noting that exploiting and comparing the two metrics defined above gave us a remarkable advantage with respect to utilizing only the model's TPM. Namely, because of the stochastic nature of the model inference, we were able to avoid the non-uniqueness issue of the TPM and, at the same time, to reliably capture the temporal characteristics of the state time courses. In fact, due to the availability of numerous scanning sessions for each subject, both

metrics could be computed not only across different subjects, but also at the individual level. We capitalized on the robustness of the HMM model inferred on HCP homogeneous data to reveal, through MP Differences and FO Correlations, temporal information of brain state time series in the heterogeneous Traveling-subject dataset. These metrics allowed us to perform a richer analysis rather than simply limiting ourselves to the study of a model's TPM—in this context it was one single matrix valid for all subjects (figure 1(a)).

## 2.5. Model selection

To select the model that best fit the data, we computed the free energy for each of the 50 different models that were inferred. The free energy provides a bound on the log-evidence for any model [47], and can be derived as the sum of the model average log-likelihood, the negative entropy, and the Kullback–Leibler divergence [48]. Because the data sets have different sizes (we used HCP<sub>1200</sub>, HCP<sub>820</sub>, and Traveling-subject only), we corrected the free energy according to the size of the dataset used for the model inference in order to compare different models fairly. Next, we ranked the  $N = 50$  models inferred in this study based on their free energy, and chose the one minimizing this quantity.

Based on previous findings [33], and because the definition of MP Difference strongly rely on the hierarchical structure of the inferred states, we also verified that the selected model presented a sufficiently marked two metastate structure. To take this topological notion into account, we computed for each model the Euclidean distance from the ideal FO Correlation Matrix (supplementary figure 2), which gauged how well the metastates emerged in the model's FO Correlation Matrix. Mathematically, this distance is defined as:

$$d_i = \left\| \mathbf{C}_i - \begin{bmatrix} \mathbf{1}_{4 \times 4} & \mathbf{0}_{4 \times 1} & -\mathbf{1}_{4 \times 7} \\ \mathbf{0}_{1 \times 4} & \mathbf{1} & \mathbf{0}_{1 \times 7} \\ -\mathbf{1}_{7 \times 4} & \mathbf{0}_{7 \times 1} & \mathbf{1}_{7 \times 7} \end{bmatrix} \right\|$$

for  $i = 1, \dots, 50$ , where  $\mathbf{C}_i$  is the FO Correlation Matrix of model  $i$ ,  $\mathbf{1}$  is a matrix of all ones,  $\mathbf{0}$  is a zero matrix, and  $\|\cdot\|$  denotes the Euclidean norm. The model that we have used in this study was not only the one with the lowest free energy, but also the one with and the smallest  $d_i$ . Thus, our model fit the data the best and simultaneously embodied a pronounced two metastate structure.

Finally, to verify the robustness of our model when applied to time series other than the HCP data, we applied the HCP-trained HMM to autoregressive data (see supplementary text and supplementary figure 3). We found that this control analysis yielded state time courses that spend most of the time on state 5. Unsurprisingly, state 5 was not only uncorrelated to all other states in our model, but had previously been found to be associated to motion artifacts in HCP

data [33]. This result substantiates the robustness of our results in regards to application of our HCP-trained model to the Traveling-subject time series.

## 2.6. Subject classification using brain dynamics fingerprints

To support our findings, and the robustness of the subject-specific fingerprints to data heterogeneity, we used machine learning on these fingerprints to perform subject-level classification. Specifically, individual subjects from the Traveling-subject dataset were classified based on their Metastate Profiles and Fractional Occupancies. We detail the procedure hereafter.

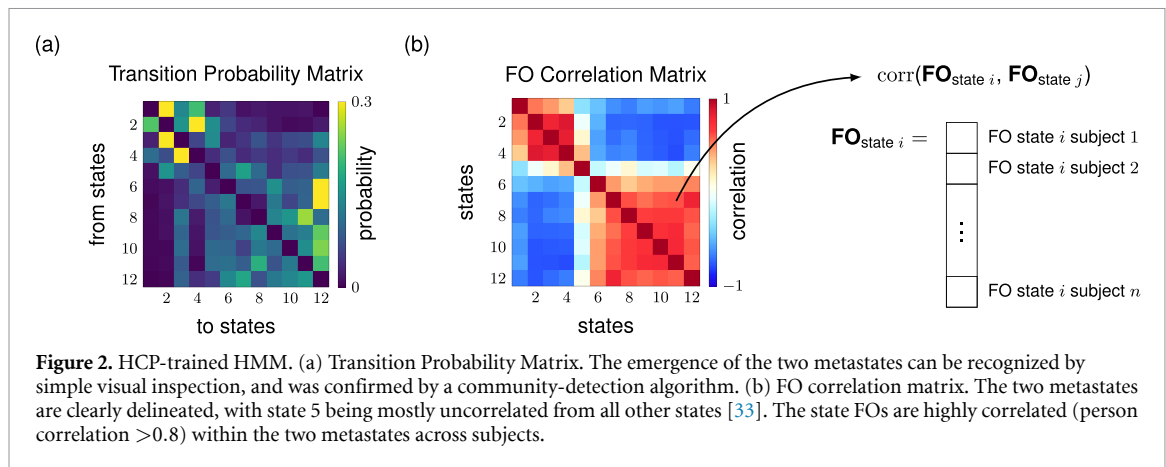
For each scanning factor, we trained a logistic regression classifier—which minimizes the cross-entropy loss—with the `scikit-learn` machine learning package [49] in Python 3 with the following parameters: default L2 penalty, default L-BFGS-B algorithm [50], and 'multi\_class' option set to 'multinomial'. The classification task was repeated multiple times by splitting the data into different training and validation sets as follows. We repeated the training and validation of the linear regression classifier for each factor attribute (e.g. for the scanner parameter, we repeated the procedure for each scanner model) by performing a leave-one-attribute-out cross-validation: we chose as validation set all the samples (i.e. fingerprints) belonging to one factor attribute, and we used as training set all the remaining samples. This analysis allowed us to (i) compare the classification based on brain dynamics fingerprints in the presence of different scanning protocols and heterogeneous data with baseline chance level, and (ii) investigate which scanning factors tend to affect data collections more than others.

## 3. Results

### 3.1. Test-retest reliability of brain dynamics estimation

We first inferred the HMM by leveraging the large amount of rs-fMRI data in the HCP dataset. Due to the stochastic nature of the HMM inference—which is based on the probabilistic process of Bayesian inference—the results might vary at each new model training. Thus, we inferred multiple models and selected for further analyses the one with the best fit. We show in figure 2 the HMM selected and employed in this work, which is the model that ranked best with respect to free energy, displayed the smallest distance from the ideal FO Correlation Matrix, and was trained solely on HCP time series (see also supplementary figure 4). Further details and matrices of notable models different from the best one can be found in supplementary figures 5–6.

Given the stochastic nature of the Variational Bayes approach used to infer the HMM [31], it was unlikely that one would obtain an exact replica of the



model originally reported in [33]. However, as displayed in figure 2(b) and supplementary figure 6, all models showed a clear two metastate structure, validating the claims that resting-state brain dynamics tend to be hierarchically organized in two larger sets of states (one associated with higher-order cognition, and the other one with sensorimotor and perceptual states, as originally reported in [33]). Moreover, a visual inspection of the TPM matrix alone suggested the emergence of two groups of states that tended to be more (statistically) connected. We confirmed this hypothesis by employing the generalized Louvain algorithm [51] for the discovery of communities in networks.

To note, we also used the HCP-derived TPM as a prior to train an HMM on the Traveling-subject dataset alone. This choice of prior ensured that the inference started from established initial conditions before dealing with the small size of the Traveling-subject dataset. Surprisingly, although the number of subjects in the Traveling-subject dataset was much smaller than the number of subjects in the HCP dataset, the two metastate structure still emerged in the model's matrices (supplementary figure 6(d)), as also confirmed by the generalized Louvain algorithm. This result highlighted that, notwithstanding mixed scanning protocols and small sample, the metastates could be retrieved and unfold as a robust feature of resting-state data.

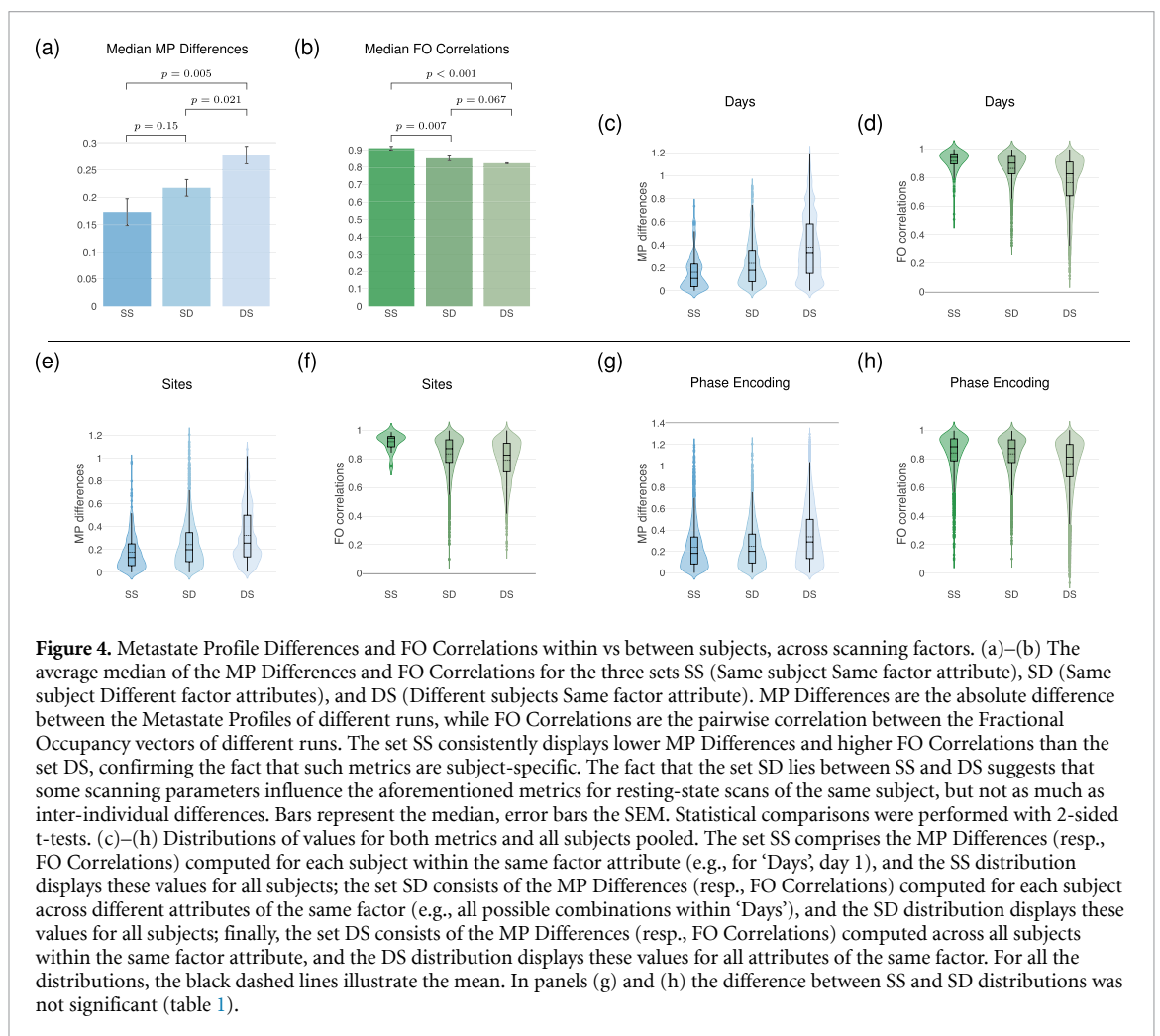
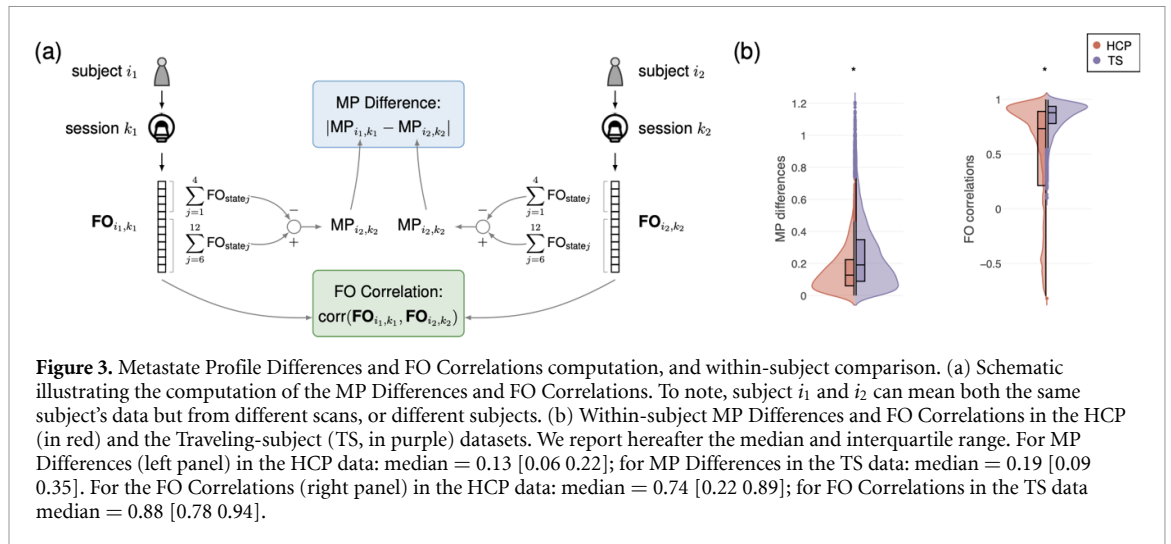
### 3.2. Metastate profiles and fractional occupancies are robust subject-specific fingerprints

Previous findings reported that brain dynamics is subject-specific and nonrandom. To extend this notion, we applied the best-fitting, HCP-trained HMM, to the Traveling-subject dataset, obtaining the state time courses for each 10 min scanning session. Next, from each individual's state time courses, we calculated the MP Differences and the FO Correlations. We summarize the derivation of these two measures in figure 3(a). To note, here we use the notation subject  $i_1$  and  $i_2$  for a general case, but this

naturally applies to two different scans belonging to the same subject (i.e. within-subject comparison).

Before delving into the main analyses of the Traveling-subject dataset, we considered the consistency of these two measures of brain activity dynamics both in the HCP and the Traveling-subjects datasets. In both datasets, there were multiple scans per subject ( $m_{\text{HCP}} = 4$  and  $m_{\text{TS}} > 42$ , respectively), allowing us to compute MP Differences and FO Correlations within subjects. Given the high homogeneity of the HCP dataset, we expected this to provide a lower bound in terms of dissimilarity between scans belonging to a given subject. Notwithstanding inherent differences (2-sample Kolmogorov-Smirnov test,  $k = 0.19$  and  $p < 10^{-3}$  for MP Differences,  $k = 0.329$  and  $p < 10^{-3}$  for FO Correlations), both MP Differences and FO Correlations distributions displayed remarkable similarity in the distributions of MP Differences (peak = 0.06 for HCP data and peak = 0.06 for TS data, figure 3(b) left plot) and FO correlations (peak = 0.9 for HCP data and peak = 0.93 for TS data, figure 3(b) right plot). Moreover, the interquartile range also had large overlap, particularly for MP Differences (figure 3(b) legend). These results provided initial evidence for the presence of—and our ability to infer—subject-specific brain dynamics patterns.

We next interrogated in detail the Traveling-subject dataset. Each scanning factor considered in this study had multiple distinct attributes. For instance, for the factor *scanner manufacturer* there were sessions recorded through scanners produced by three different manufacturers (Siemens, Philips, and General Electric, see also supplementary table 1). We computed the values of MP Differences and FO Correlations for all the runs of the same subject and the same factor attribute (SS), the same subject and different factor attributes (SD), and different subjects but the same factor attribute (DS). A 1-way ANOVA on the median MP Differences (figure 4(a)), and on the median FO Correlations (figure 4(b)), resulted in a highly significant main effect of comparison group (SS, SD, DS), for both



measures (MP Differences:  $F_{2,15} = 7.64$ ,  $p = 0.005$ ; FO Correlations:  $F_{2,15} = 19.76$ ,  $p < 10^{-3}$ ). Applying post-hoc comparisons, we found that, on average, the median MP Differences for the same subject within the same factor (SS) were significantly lower than the median MP Differences for different subjects within the same factor (DS), ( $\sim 38\%$  lower, 2-sided

$t$ -test,  $t_{10} = -3.59$ ,  $p = 0.005$ , figure 4(a)). Analogously, on average, the median FO Correlations within the same factor for the same subject were higher than across different subjects ( $\sim 10\%$  higher, 2-sided  $t$ -test,  $t_{10} = 8.15$ ,  $p < 10^{-3}$ , figure 4(b)). Additional evidence for how the state time courses of a given subject (within the same factor attributes) tended to be

particularly similar was also evident in the FO Correlations median values of the group SS being significantly higher than the median FO Correlations in the groups SD and DS (figure 4(b)). These findings support the hypothesis that MP Differences and FO Correlations are robust subject-specific measures, as they were resilient to the single effect of all the factors considered in this study.

To further substantiate these results, we used a simple machine learning approach to predict individuals based on their brain dynamics fingerprints. We applied logistic regression to classify the individuals in the Traveling-subject dataset by a leave-one-attribute-out cross-validation procedure (section 2). In brief, for each factor, we repeated the training and validation of the classifier as many times as the number of factor attributes, using each time the samples of one left-out factor attribute as validation set and the remaining samples from all other attributes as training set. We found the accuracy of the classification to be consistently well above the theoretical chance level (9 subjects:  $1/9 \approx 0.11$ ), scoring on average  $0.22 \pm 0.02$  for the classification based on MPs (a single value for each factor attribute) ( $t$ -test against chance level,  $t_5 = 16.4$ ,  $p < 10^{-4}$ ),  $0.30 \pm 0.03$  for the classification based on FOs (a length-11 vector for each factor attribute) ( $t$ -test against chance level,  $t_5 = 17.62$ ,  $p < 10^{-3}$ ), and  $0.28 \pm 0.02$  when using the combined measures ( $t$ -test against chance level,  $t_5 = 21.56$ ,  $p < 10^{-3}$ ). We report the classification results for each factor in see supplementary table 3 (see also supplementary figure 7).

### 3.3. In rs-fMRI data, not all factors are equal

Given that the Traveling-subject dataset contained a considerable number of factors, we inquired which of these factors, and to what extent, influenced the subject-specific fingerprints defined on the HMM state time courses. Specifically, we asked which factors affected the MP Differences and the FO Correlations most, both within and across subjects. Thus, we compared three different groups (SS, SD, and DS, as illustrated in figure 1(b)) of MP Differences and FO Correlations, for six different factors, each containing at least two attributes (see supplementary table 1 for the full list of factors and associated attributes).

Although different runs always carried some variability, some factors seemed to influence the MP Differences and the FO Correlations more than inherent inter-subject differences. We summarize the main results of this comparison in figure 4 and report the additional ones in supplementary figure 8. We also report in table 1 the results of Kolmogorov-Smirnov nonparametric tests between all the distributions of values for the groups of MP Differences and FO Correlations. More in detail, by comparing the distributions of values for both metrics between the sets SS (Same subject and Same factor attribute) and SD (Same subject and Different factor attributes), we

**Table 1.** 2-Sample Kolmogorov-Smirnov test results for MP Differences and FO Correlations. The check-mark indicates that the difference is significant (i.e. the null hypothesis that the samples are drawn from the same underlying continuous population can be rejected at the 5% significance level), and the cross otherwise. All  $p$ -values have been FDR-adjusted [52] and they all satisfy  $p < 10^{-3}$  when the null hypothesis is rejected. Test statistics are reported in supplementary table 2. SS: Same subject Same factor attribute. SD: Same subject Different factor attributes. DS: Different subjects Same factor attribute.

Factor	MP Diff.		FO Corr.	
	SS	SD	SS	SD
	vs	vs	vs	vs
	SD	DS	SD	DS
1. Site	✓	✓	✓	✓
2. Day	✓	✓	✓	✓
3. Phase	✗	✓	✗	✓
4. Channels/coil	✓	✓	✓	✓
5. Manufacturer	✓	✓	✓	✓
6. Scanner	✓	✓	✓	✗

found them to be statistically different ( $p < 10^{-3}$ , see table 1) for all factors except for the phase encoding direction, as also noticeable in figures 4(g) and (h). It is worth noting that the median MP Difference of any given subject displayed only small changes in the comparison within attribute vs between attributes for all factors (2-sided  $t$ -test,  $t_{10} = -1.55$ ,  $p = 0.15$ ); compatibly, the median FO Correlations were, on average,  $\sim 6.5\%$  higher in the group SS than in the group SD (2-sided  $t$ -test,  $t_{10} = 3.43$ ,  $p = 0.007$ ).

Additionally, the machine learning classifications of brain dynamics fingerprints described earlier were qualitatively generally in agreement with these findings. Leave-one-attribute-out classification revealed that, for both fingerprints, the accuracy in predicting individual subjects was the lowest when the training and validation sets were based on different days (see supplementary table 3).

To further evaluate the influence that different scanning variables have on MP Differences and FO Correlations, we directly compared their effects across these fingerprints. We first analyzed the raw medians of the distributions of MP Differences and FO Correlations for each scanning factor in the groups SS (Same subject Same factor attribute), SD (Same subject Different factor attributes), and DS (Different subjects Same factor attribute). We found that, while both fingerprints possessed a shared variance (figure 5(a), Coefficient of determination  $R^2 = 0.375$ ), they also provided independent information. In fact, as evident not only by their distributions of values in figure 4, MP Differences displayed consistently larger median differences within the three groups of values (SS, SD, DS) than FO Correlations (figure 5(a), 2-sided Wilcoxon signed rank test,  $z = 3.68$ ,  $p < 10^{-3}$ ).

Next, to achieve an unbiased estimate of the effect size of each factor on the distributions of MP Differences and FO Correlations, we computed the

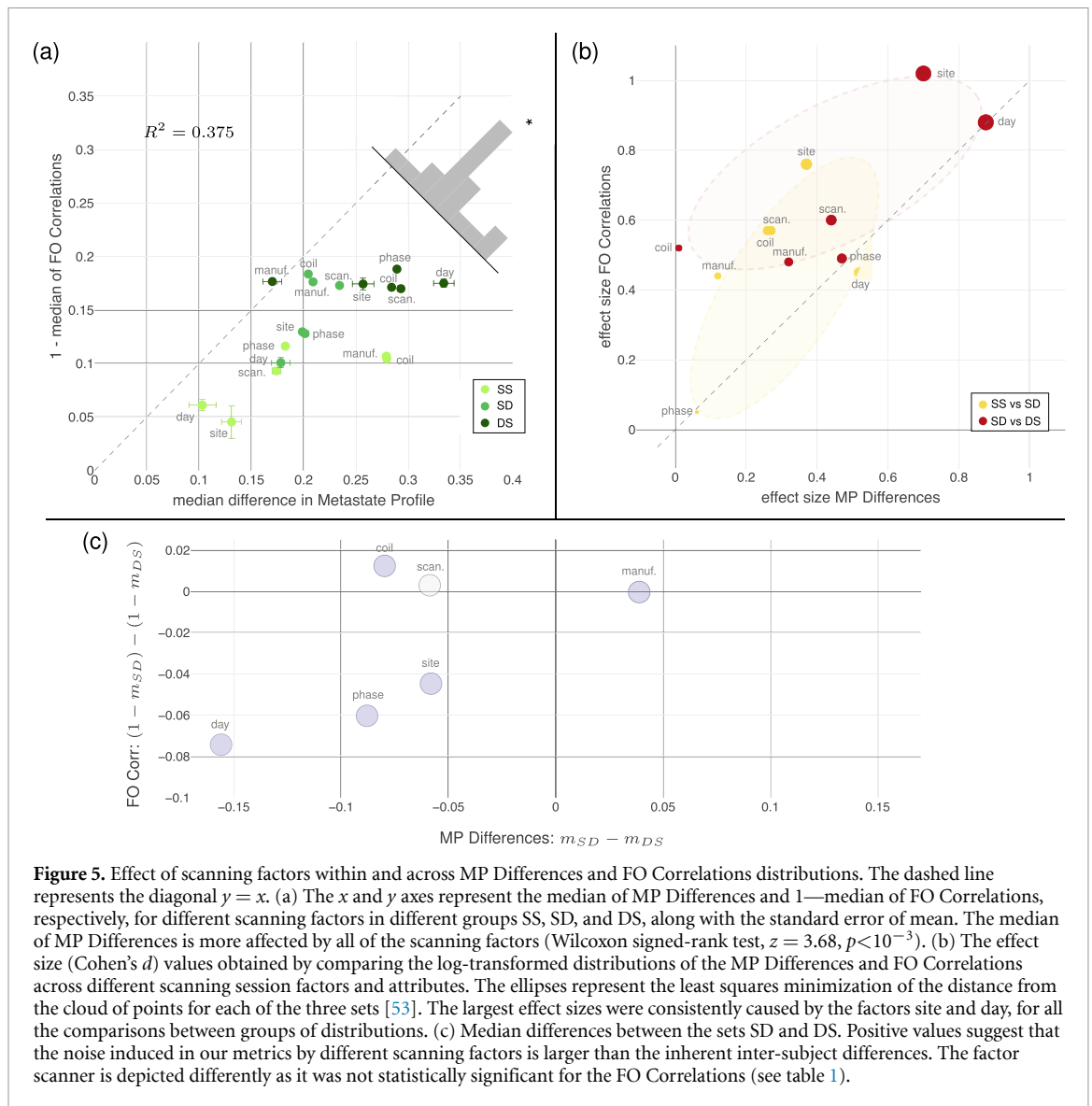


**Figure 5.** Effect of scanning factors within and across MP Differences and FO Correlations distributions. The dashed line represents the diagonal  $y = x$ . (a) The x and y axes represent the median of MP Differences and 1—median of FO Correlations, respectively, for different scanning factors in different groups SS, SD, and DS, along with the standard error of mean. The median of MP Differences is more affected by all of the scanning factors (Wilcoxon signed-rank test,  $z = 3.68$ ,  $p < 10^{-3}$ ). (b) The effect size (Cohen's  $d$ ) values obtained by comparing the log-transformed distributions of the MP Differences and FO Correlations across different scanning session factors and attributes. The ellipses represent the least squares minimization of the distance from the cloud of points for each of the three sets [53]. The largest effect sizes were consistently caused by the factors site and day, for all the comparisons between groups of distributions. (c) Median differences between the sets SD and DS. Positive values suggest that the noise induced in our metrics by different scanning factors is larger than the inherent inter-subject differences. The factor scanner is depicted differently as it was not statistically significant for the FO Correlations (see table 1).

Cohen's  $d$  from the log-transformed distributions of the MP Differences and FO Correlations across all scanning factors, between groups SS-SD and SD-DS. Figure 5(b) highlights how the dissimilarity between brain dynamics fingerprints was the greatest when comparing, for the same scanning factor, measures from the same subject and measures from different subjects. Based on this observation, we assessed which scanning factors influenced the median values of the groups SD and DS the most by computing  $m_{SD} - m_{DS}$ , where  $m$  denoted the median, for the MP Differences, and  $(1 - m_{SD}) - (1 - m_{DS})$  for the FO Correlations. Notice that a positive value indicates that the noise induced by different factors (group SD) has a larger effect than than inter-subject differences (group DS). In accordance with the analysis above, we found that most of the scanning factors seemed to induce less noise on our metrics than the inter-subject differences. Therefore, while site and day were the co-variate associated with the largest effect in the two groups SS vs SD and SD vs DS (figure 5(b)), the

results in figure 5(c) suggest that the number of coils and the manufacturer are the only factors for which we can robustly estimate the effect on the data, beyond inter-subject differences.

#### 4. Discussion

In this work, we addressed the issues of reproducibility and variability of fMRI data from the angle of brain dynamics. We leveraged the large HCP collection of rs-fMRI data to infer a HMM capable of describing brain state time courses at the subject level. By applying such a model to a dataset of traveling subjects, we found that brain network dynamics displayed signature fingerprints that were robust to different physical and temporal factors affecting the data that populates multi-site collections of neuroimaging data. Precisely, we found that MP Differences and FO Correlations are reliable, stable individual traits, as shown by the SS/DS differences, when taken across all factors (figures 4(a) and (b)). This study corroborates

and complements previous work that found that the emergence of temporal patterns of brain activity tend to repeat more similarly within the same subject and over time [28, 33, 54]. This result promotes further investigations on the dynamical characteristics of brain states.

Recent years have witnessed a growing interest in the identification and characterization of the factors that tend to introduce spurious effects in multi-site fMRI recordings, endangering the reproducibility and the overall quality of the results that may be inferred from these data. The first warnings came from a study that investigated sources of nuisance variation across multiple sites and their impact on rs-fMRI data [23], followed by a number of studies that reported mostly consistent results [14–16, 19, 20]. Although we used different methods, our finding that different scanning factors introduce noise into brain dynamics fingerprints (as can be seen by the SS/SD comparisons in figure 5(b)) is in line with prior reports [16, 19]. Furthermore, the present study made use of larger datasets. The Traveling-subject dataset contains the largest number of subjects out of all the aforementioned studies. To date, only [16] has more sites than the Traveling-subject dataset used in this study, but it has the drawback of scanning only a single subject. The Traveling-subject dataset also allowed for the analysis of some scanning factors—such as the numbers of channels per coil or different scanner models within the same vendor—that have not been taken into consideration in previous work, giving more breadth and depth to our findings. Nevertheless, it is important to stress out that the potential variability brought in by scanning factors may not always be a necessarily negative feature. In fact, such variability may even be a powerful test for reproducibility of some findings. For instance, although different scanning factors may be confounds for certain analyses (e.g. comparing participant populations from different sites), they can also be used to test the robustness of a model when generalizing analyses across sites with different scanning parameters. Our results complement, from a dynamical point of view, both seminal and more recent work reporting more dissimilar resting-state networks inter-subject than intra-subject [16, 23, 39, 55].

Functional connectivity—typically computed as the correlation between time series representing the average activity in a brain region—has been the mainstay in the analysis of variability in fMRI data. Previous work has demonstrated that a sizable amount of recordings from the same site enables precise measurements of individual variations in functional connectivity [39], and that individual differences in functional networks are not affected by anatomical misalignment [55]. Here, we complement such studies by showing that individual signatures can still be (easily) recovered within limited recordings from multiple sites (i.e. in the Traveling-subject dataset).

To note, the comparison of functional connectivity between scanning sessions is inherently different from the comparison of state time courses. Differently from functional connectivity computed over a whole scanning session, the HMM captures the local temporal wandering of brain activity across states (networks). Therefore, while comparing functional connectivity between different subjects may be akin to comparing longer-term traits, comparing state time courses between subjects may be more closely aligned to comparing a repetition of sequences of brain states at rest.

While the aforementioned studies on functional connectivity have significantly increased our understanding of the brain as a system that obeys network-wide principles, they are mainly agnostic to temporal dynamics within the scanning sessions. This may prevent the level of precision that could at times be the most clinically relevant [56]. Differently from [16, 20], where time seemed to play a negligible effect, we found that different scanning days greatly affected our estimation of brain network dynamics. As mentioned earlier, an intuitive explanation for this apparent discrepancy is that functional connectivity tends to be associated to more coarsely defined subjective traits, whereas an HMM, being inherently more sensitive to temporal differences, is apt to capture more instantaneous cognitive processes. It is worth noting that our findings do not go against the claim that functional connectivity networks remain a reliable subject-specific fingerprint over long period of times, but rather we suggest that brain state trajectories can differ extensively between days, probably due to different cognitive or mental processes. As such, we suggest that dynamic and static measures in fact carry complementary information, which may provide additional insight when used in combination. However, due the limited number of scanning sessions taken on different days in the Traveling-subject dataset (see supplementary table 1), and to the inter-subject variability being larger than the variability across different factors (see figure 5(c)), future studies will need to further validate this fact.

How do HMMs compare with the sliding window approach? The sliding window analysis is typically used to improve the temporal definition of functional connectivity studies [57]. Albeit being intrinsically easier to set up, it has crucial limitations. Namely, the sliding window size is constrained by a trade-off between time resolution and quality of the results, and the conclusions from sliding window studies tend to be affected by sampling variability [58]. Conversely, HMM is as fast as the data modality allows, since it provides instantaneous likelihood of high correlation between brain signals [33].

If the goal of a study is a robust and detailed description of a system's dynamics, the HMM approach requires large amounts of data for training purposes, thus appearing not suitable to analyze

small cohorts of subjects. However, in this study we give proof-of-concept that one can use a very large dataset (i.e. HCP) to infer an HMM, which can then be applied to a smaller dataset. Our results indicate that this procedure is robust. Interestingly, if only a relatively small number of subjects is available for the inference process, it is still possible to recover a coarser—and nonrandom—representation of the brain dynamics by using the TPM inferred from a large dataset as a prior (see supplementary figure 6(d)). Thus, detailed analyses and claims based on HMM should be gauged on the size of the available data. This is a common requirement in neuroimaging studies, as functional connectivity studies also require large amount of data to enable precise measurements [39].

Despite its capabilities, HMM is based on some premises (see also [31, 33] for thorough discussions). It is worth noting that the HMM builds on the Markovian assumption, theorizing that we can predict, based on the state we are at time  $t$ , which state is more likely to follow at time  $t + 1$ . Yet, while the brain may violate this assumption due to established long-range temporal dependencies [4], FO Correlations and MP Differences inherently display information that appears at longer time scales.

There are some limitations to this work. For example, while the decoding approach utilized here—training the HMM on the HCP data, and infer brain states trajectories in the Traveling-subject dataset, is a strength of this study, it is also one of its limitations. The HCP and Traveling-subject datasets harbor some differences relating to the scanning protocols or even the countries in which the data were collected (US and Japan). For instance, the sampling rate of the two datasets were originally different ( $TR_{\text{HCP}} = 0.72$  s and  $TR_{\text{TS}} = 2.5$  s). As such, the up-sampling of the Traveling-subject dataset may have been sub-optimal and thus bias the overall HMM-based brain state dynamics estimation. Yet, the presence of these very differences appear to corroborate the finding that brain dynamics fingerprints are subject-specific. Specifically, we still find that, on average, the MP Differences (resp., FO Correlations) are lower (resp., higher) within subjects than across subjects, even when comparing runs with different scanning parameters. The fact that, at the within-subject level, these two measures had very similar values to those obtained from the HCP dataset (where both model and fingerprints were derived from the same data) provides strong support for this interpretation (i.e. brain dynamics fingerprints are subject-specific), such that it is unlikely that these results are due to inherent bias or noise. A second limitation may arise from the factors that were considered in the traveling-subject dataset. Although there are several factors, some with many attributes (e.g. there are 12 sites), these factors are sometimes nested within each other. For instance, within the same phase encoding

attribute there are scans belonging to different sites. This aspect may have partly influenced (reduced) the effect size of such factors which are heterogeneous with respect to *other* factors, while factors such as day or site would remain unaffected, since these scans were recorded at the same site, with the same protocol. Above all, while the Traveling-subject dataset allowed us to investigate the nuisance effect of multiple variables, it did not offer any insight into other relevant scanning factors such as TR length, the duration of the scanning session, and voxel sizes. To enhance our collective appraisal of the sources of variability in heterogeneous collections of rs-fMRI data, it will be important to generate datasets that include variations along these additional dimensions.

Given the considerable recent advances in inference techniques [31, 59, 60], and the ever-increasing availability of computational power, our work further suggests that the HMM is, and, most importantly, will be, a powerful technique to explain and interpret the dynamic aspects of the brain. Furthermore, the possibility of inferring an HMM on a very large dataset to apply it to a much smaller one has important implications for clinical applications. In the future, perhaps with even more data, these general models could be built and then utilized to infer subject-specific fingerprints in other smaller cohorts and be used for a more personalized approach to treatments. In other words, a one-size-fits-all approach could be employed to build the model in its general terms, consequently allowing us to move to a personalized course of action by evaluating the model at the individual level. For instance, closed-loop fMRI neurofeedback [61, 62] could significantly benefit from these models, which will allow for a more holistic approach to the dynamical properties of mental and cognitive processes, particularly from a clinical perspective [37, 56, 63, 64].

## 5. Conclusion

In this work, we address the important issues of reproducibility and variability of fMRI data. We leveraged the large, homogeneous HCP collection of resting-state data to reliably infer a HMM capable of describing the brain state time courses at the subject level. By applying such a model to a dataset of traveling subjects, we show that dynamical states can be estimated reliably. Specifically, we find that brain network dynamics displays fingerprints that are robust to different scanning factors and distinctive for each subject. Further, we explore which scanning factors impact measures of brain dynamics the most, and what is the magnitude of their effect. We find that, amongst the scanning factors available in our dataset, sites and days tend to induce higher variability in the estimation of individual brain state time courses. However, due to the large noise induced by inter-subject variability and the limited sample size, this claim will need further validation by future studies.

These results enable and promote further investigations on the dynamical characteristics of brain states. Once a good model is inferred, it can be applied to a battery of different goals, such as the analysis of task-based datasets, the examination of data collections from subjects with neurological disorders, and the promising use in clinical or rehabilitation settings, for instance by using brain state inference in clinical populations to estimate the best time for providing a given treatment.

## Acknowledgments

We thank the Washington University–University of Minnesota Consortium of the Human Connectome Project (WU-Minn HCP) for generating and making publicly available the HCP data. Data used in the preparation of this work were obtained from the DecNef Project Brain Data Repository (<https://bicr-resource.atr.jp/srpbsts/>) gathered by a consortium as part of the Japanese Strategic Research Program for the Promotion of Brain Science (SRPBS) supported by the Japanese Advanced Research and Development Programs for Medical Innovation (AMED). T.M. is supported by the National Science Foundation (NSF) (USA, Grant NCS-FO-1631112), by the Army Research Office (ARO) (USA, Grant ARO-71603NSYIP), by JST ERATO (Japan, Grant JPMJER1801), and by AMED (Japan, Grant JP18dm0307008). G.L. is supported by AMED (Japan, Grant JP18dm0307002). A.C. is supported by JST ERATO (Japan, Grant JPMJER1801) and by AMED (Japan, Grants JP18dm0307002 and JP18dm0307008).

## ORCID iDs

Tommaso Menara  <https://orcid.org/0000-0002-5523-2170>

Fabio Pasqualetti  <https://orcid.org/0000-0002-8457-8656>

Aurelio Cortese  <https://orcid.org/0000-0003-4567-0924>

## References

- [1] Raichle M E, MacLeod A M, Snyder A Z, Powers W J, Gusnard D A and Shulman G L 2001 A default mode of brain function *Proc. Natl Acad. Sci.* **98** 676–82
- [2] Damoiseaux J S et al 2006 Consistent resting-state networks across healthy subjects *Proc. Natl Acad. Sci.* **103** 13848–53
- [3] Allen E A, Damaraju E, Plis S M, Erhardt E B, Eichele T and Calhoun V D 2012 Tracking whole-brain connectivity dynamics in the resting state *Cereb. Cortex* **24** 663–76
- [4] He B J 2011 Scale-Free properties of the functional magnetic resonance imaging signal during rest and task *J. Neurosci.* **31** 13786–95
- [5] Zalesky A, Fornito A, Cocchi L, Gollo L L and Breakspear M 2014 Time-resolved resting-state brain networks *Proc. Natl Acad. Sci.* **111** 10341–6
- [6] Smith S M et al 2013 Resting-state fMRI in the human connectome project *NeuroImage* **80** 144–68
- [7] Van Essen D C, Smith S M, Barch D M, Behrens T E J, Yacoub E and Ugurbil K 2013 The WU-minn human connectome project: an overview *NeuroImage* **80** 62–79
- [8] Sudlow C et al 2015 UK biobank: an open access resource for identifying the causes of a wide range of complex diseases of middle and old age *PLoS Med.* **12** 1–10
- [9] Jack J C R et al 2008 The Alzheimer's disease neuroimaging initiative (ADNI): MRI methods *J. Magn. Reson. Imaging* **27** 685–91
- [10] Yahata N et al 2016 A small number of abnormal brain connections predicts adult autism spectrum disorder *Nat. Commun.* **7** 1–12
- [11] Drysdale A T et al 2017 Resting-state connectivity biomarkers define neurophysiological subtypes of depression *Nat. Med.* **23** 28–38
- [12] Abraham A et al 2017 Deriving reproducible biomarkers from multi-site resting-state data: an Autism-based example *NeuroImage* **147** 736–45
- [13] Varoquaux G and Craddock R C 2013 Learning and comparing functional connectomes across subjects *NeuroImage* **80** 405–15
- [14] Poldrack R A, Whitaker K and Kennedy D 2019 Introduction to the special issue on reproducibility in neuroimaging *NeuroImage* **218** 116357
- [15] Bari S, Amico E, Vike N, Talavage T M and Goñi J 2019 Uncovering multi-site identifiability based on resting-state functional connectomes *NeuroImage* **202** 115967
- [16] Badhwar A et al 2020 Multivariate consistency of resting-state fMRI connectivity maps acquired on a single individual over 2.5 years, 13 sites and 3 vendors *NeuroImage* **205** 116210
- [17] Feis R A et al 2015 ICA-based artifact removal diminishes scan site differences in multi-center resting-state fMRI *Front. Neurosci.* **9** 395
- [18] Jann K et al 2015 Functional connectivity in BOLD and CBF data: similarity and reliability of resting brain networks *NeuroImage* **106** 111–22
- [19] Noble S et al 2017 Multisite reliability of MR-based functional connectivity *NeuroImage* **146** 959–70
- [20] Hawco C et al 2018 A longitudinal human phantom reliability study of multi-center T1-weighted, DTI and resting state fMRI data *Psychiatry Res. Neuroimaging* **282** 134–42
- [21] Fortin J P et al 2018 Harmonization of cortical thickness measurements across scanners and sites *NeuroImage* **167** 104–20
- [22] Yamashita A et al 2019 Harmonization of resting-state functional MRI data across multiple imaging sites via the separation of site differences into sampling bias and measurement bias *PLOS Biol.* **17** 1–34
- [23] Yan C G, Craddock R C, Zuo X N, Zang Y F and Milham M P 2013 Standardizing the intrinsic brain: towards robust measurement of inter-individual variation in 1000 functional connectomes *NeuroImage* **80** 246–62
- [24] Friston K J 1997 Transients, metastability and neuronal dynamics *NeuroImage* **5** 164–71
- [25] Faure P and Korn H 2001 Is there chaos in the brain? I. concepts of nonlinear dynamics and methods of investigation *Comptes Rendus de l'Acad. Sci.* **III** **324** 773–93
- [26] Markram H 2006 The blue brain project *Nat. Rev. Neurosci.* **7** 153
- [27] Bansal K, Medaglia J D, Bassett D S, Vettel J M and Muldoon S F 2018 Data-driven brain network models differentiate variability across language tasks *PLOS Computat. Biol.* **14** 1–25
- [28] Vidaurre D et al 2018 Spontaneous cortical activity transiently organises into frequency specific phase-coupling networks *Nat. Commun.* **9** 2987
- [29] Singh M F, Braver T S, Cole M W and Ching S 2020 Estimation and validation of individualized dynamic brain models with resting state fMRI *NeuroImage* **221** 117046

- [30] Varoquaux G and Thirion B 2014 How machine learning is shaping cognitive neuroimaging *GigaScience* **3** 28
- [31] Vidaurre D et al 2018 Discovering dynamic brain networks from big data in rest and task *Neuroimage* **180** 646–56
- [32] Kaufmann T et al 2019 Common brain disorders are associated with heritable patterns of apparent aging of the brain *Nat. Neurosci.* (available at: [www.nature.com/articles/s41593-019-0471-7](http://www.nature.com/articles/s41593-019-0471-7))
- [33] Vidaurre D, Smith S M and Woolrich M W 2017 Brain network dynamics are hierarchically organized in time *Proc. Natl Acad. Sci.* **114** 12827–32
- [34] Lotte F et al 2018 A review of classification algorithms for EEG-based brain–computer interfaces: a 10 year update *J. Neural Eng.* **15** 031005
- [35] Lisi G, Rivela D, Takai A and Morimoto J 2018 Markov switching model for quick detection of event related desynchronization in EEG *Front. Neurosci.* **12** 24
- [36] Mitchell T J et al 2013 A novel data-driven approach to preoperative mapping of functional cortex using resting-state functional magnetic resonance imaging *Neurosurgery* **73** 969–83
- [37] Stiso J et al 2019 White matter network architecture guides direct electrical stimulation through optimal state transitions *Cell Rep.* **28** 2554–66.e7
- [38] Charquero-Ballester M et al 2020 Effective psychological treatment for PTSD changes the dynamics of specific large-scale brain networks bioRxiv (available at: [www.biorxiv.org/content/early/2020/01/07/2020.01.07.891986](http://www.biorxiv.org/content/early/2020/01/07/2020.01.07.891986))
- [39] Gratton C et al 2018 Functional brain networks are dominated by stable group and individual factors, not cognitive or daily variation *Neuron* **98** 439–52
- [40] Smith S M et al 2013 Functional connectomics from resting-state fMRI *Trends Cogn. Sci.* **17** 666–82
- [41] Glasser M F et al 2013 The minimal preprocessing pipelines for the Human Connectome project *Neuroimage* **80** 105–24
- [42] Griffanti L et al 2014 ICA-based artefact removal and accelerated fMRI acquisition for improved resting state network imaging *NeuroImage* **95** 232–47
- [43] Ciric R et al 2017 Benchmarking of participant-level confound regression strategies for the control of motion artifact in studies of functional connectivity *NeuroImage* **154** 174–87
- [44] Power J D, Barnes K A, Snyder A Z, Schlaggar B L and Petersen S E 2012 Spurious but systematic correlations in functional connectivity MRI networks arise from subject motion *NeuroImage* **59** 2142–54
- [45] Yan C G, Wang X D, Zuo X N and Zang Y F 2016 DPABI: data processing analysis for (resting-state) brain imaging *Neuroinformatics* **14** 339–51
- [46] Vidaurre D, Quinn A J, Baker A P, Dupret D, Tejero-Cantero A and Woolrich M W 2016 Spectrally resolved fast transient brain states in electrophysiological data *Neuroimage* **126** 81–95
- [47] Friston K, Mattout J, Trujillo-Barreto N, Ashburner J and Penny W 2007 Variational free energy and the laplace approximation *NeuroImage* **34** 220–34
- [48] Rezek I, Roberts S Husmeier D, Dybowski R and Roberts S (eds) 2005 *Ensemble Hidden Markov Models with Extended Observation Densities for Biosignal Analysis* (London: Springer) pp 419–50
- [49] Pedregosa F et al 2011 Scikit-learn: machine learning in python *J. Mach. Learn. Res.* **12** 2825–30
- [50] Zhu C, Byrd R H, Lu P and Nocedal J 1997 Algorithm 778: L-BFGS-B: fortran subroutines for large-scale bound-constrained optimization *ACM Trans. Math. Softw.* **23** 550–60
- [51] Blondel V D, Guillaume J L, Lambiotte R and Lefebvre E 2008 Fast unfolding of communities in large networks *J. Stat. Mech.: Theory Exp.* **2008** 10008
- [52] Yekutieli D and Benjamini Y 1999 Resampling-based false discovery rate controlling multiple test procedures for correlated test statistics *J. Stat. Plan. Inference* **82** 171–96
- [53] Haltr R and Flusser J 1998 Numerically stable direct least squares fitting of ellipses *Proc. 6th Int. Conf. in Central Europe on Computer Graphics and Visualization*. WSCG vol 98 Citeseer pp 125–32
- [54] Curtis C E and D’Esposito M 2003 Persistent activity in the prefrontal cortex during working memory *Trends Cogn. Sci.* **7** 415–23
- [55] Gordon E M, Laumann T O, Adeyemo B and Petersen S E 2015 Individual variability of the system-level organization of the human brain *Cereb. Cortex* **27** 386–99
- [56] Chiba T et al 2020 A reciprocal inhibition model of alternations between under-/overemotional modulatory states in patients with PTSD *Mol. Psychiatry* 1–17
- [57] Lurie D J et al 2019 Questions and controversies in the study of time-varying functional connectivity in resting fMRI *Netw. Neurosci.* **4** 30–69
- [58] Hindriks R et al 2016 Can sliding-window correlations reveal dynamic functional connectivity in resting-state fMRI? *NeuroImage* **127** 242–56
- [59] Bonomi M, Camilloni C, Cavalli A and Vendruscolo M 2016 MetaInference: a Bayesian inference method for heterogeneous systems *Sci. Adv.* **2** e1501177
- [60] Bzdok D and Yeo B T T 2017 Inference in the age of big data: future perspectives on neuroscience *NeuroImage* **155** 549–64
- [61] Cortese A, Amano K, Koizumi A, Kawato M and Lau H 2016 Multivoxel neurofeedback selectively modulates confidence without changing perceptual performance *Nat. Commun.* **7** 1–18
- [62] Taschereau-Dumouchel V, Cortese A, Lau H and Kawato M 2020 Conducting decoded neurofeedback studies *Soc. Cogn. Affective Neurosci.* **Nsaa063**
- [63] Taschereau-Dumouchel V, Cortese A, Chiba T, Knotts J D, Kawato M and Lau H 2018 Towards an unconscious neural reinforcement intervention for common fears *Proc. Natl Acad. Sci.* **115** 3470–5
- [64] Stoeckel L E et al 2014 Optimizing real time fMRI neurofeedback for therapeutic discovery and development *NeuroImage Clin.* **5** 245–55